

---

# PROPRIOCEPTIVE LEARNING WITH SOFT POLYHEDRAL NETWORKS\*

---

A PREPRINT

**Xiaobo Liu, Xudong Han**

Department of Mechanical and Energy Engineering  
Southern University of Science and Technology  
Shenzhen, China 518055

**Wei Hong**

Department of Mechanics and Aerospace Engineering  
Southern University of Science and Technology  
Shenzhen, China 518055

**Fang Wan\***

School of Design  
Southern University of Science and Technology  
Shenzhen, China 518055  
wanf@sustech.edu.cn

**Chaoyang Song\***

Department of Mechanical and Energy Engineering  
Southern University of Science and Technology  
Shenzhen, China 518055  
songcy@ieee.org

August 17, 2023

## ABSTRACT

Proprioception is the “sixth sense” that detects limb postures with motor neurons. It requires a natural integration between the musculoskeletal systems and sensory receptors, which is challenging among modern robots that aim for lightweight, adaptive, and sensitive designs at a low cost. Here, we present the Soft Polyhedral Network with an embedded vision for physical interactions, capable of adaptive kinesthesia and viscoelastic proprioception by learning kinetic features. This design enables passive adaptations to omni-directional interactions, visually captured by a miniature high-speed motion tracking system embedded inside for proprioceptive learning. The results show that the soft network can infer real-time 6D forces and torques with accuracies of 0.25/0.24/0.35 N and 0.025/0.034/0.006 Nm in dynamic interactions. We also incorporate viscoelasticity in proprioception during static adaptation by adding a creep and relaxation modifier to refine the predicted results. The proposed soft network combines simplicity in design, omni-adaptation, and proprioceptive sensing with high accuracy, making it a versatile solution for robotics at a low cost with more than 1 million use cycles for tasks such as sensitive and competitive grasping, and touch-based geometry reconstruction. This study offers new insights into vision-based proprioception for soft robots in adaptive grasping, soft manipulation, and human-robot interaction.

**Keywords** Soft Robotics · Force and Tactile Sensing · In-finger Vision · Proprioception

## 1 Introduction

Human fingers are dexterously adaptive in handling physical interactions through the bodily neuromuscular sense of proprioception expressed in multiple modalities. The neurological mechanism of proprioception is to sense from within, involving a complex of receptors for position and movement, as well as force and effort [Taylor, 2009]. Although rich literature has been devoted to the research of artificial skins [You et al., 2020, Li et al., 2022a, Wang et al., 2021] and robotic end-effectors [Lee et al., 2020, Odhner et al., 2014, Zhang et al., 2022, Sun et al., 2021], design integration of the two into a coherent robot system remains a challenge. The mechanical properties of human skin affect the activation of receptive organs, among which viscoelasticity is one of the most critical factors that are difficult to model [Joodaki and Panzer, 2018], resulting in time-dependent nonlinear behaviors [Parvini et al., 2022, Malhotra et al., 2019, Wang

---

\* A preprint submitted to the **International Journal of Robotics Research** for review.

**Table 1: A comparison between state-of-the-art soft sensory fingers and fingertips and our design.**

Sensor	Sensing Method	Geometric Adaptation	Compression Force Range	Precision in Relative Error
GelSight [Yuan et al., 2017]	Internal Vision	Regional at the Fingertip	~25.0 N	~2.7%
Insight [Sun et al., 2022]	Internal Vision	Regional as a Finger	2.0 N	~1.5%
Soft Continuum Finger [Thuruthel et al., 2019]	Strain Sensor	Global as a Finger	~0.35 N	15.3%
Fin Ray Finger (FRE) Model [Shan and Birglen, 2020]	Theoretical Model Only	Global as a Finger	~50.0 N	~13.7%*
FRE w/ External Vision [Xu et al., 2021]	External Vision	Global as a Finger	3.0 N	6.5%
<b>Soft Polyhedral Network (Ours)</b>	Internal Vision	Global as a Finger	20.0 N	<b>1.25%</b>

\*Precision of the theoretical model proposed in [Shan and Birglen, 2020], not a precision for sensing.

and Hayward, 2007]. With a growing trend in building soft robotic systems, designing soft fingers with proprioception extends the robot’s adaptive intelligence while interacting with the physical world or human operators.

We present the Soft Polyhedral Networks capable of vision-based proprioception with passive adaptations in omnidirections, significantly extending our previous work on vision-based tactile sensing with the soft robotic network [Wan et al., 2022]. The design method transforms any polyhedral geometry into a soft network with mechanically programmable adaptation under passive interaction. In this study, we choose a particular design variation for robotic finger integration. By adding a miniature motion capture system to the base, we accurately captured and encoded the soft network’s whole-body deformation in real-time by tracking the spatial movement of a fiducial marker attached inside. This allows us to quantitatively study the viscoelasticity in the soft metamaterial, which is usually ignored in soft robotics. To model the non-negligible viscoelasticity of the soft network for dynamic proprioception, we encode both deformation and kinetic input features to learn a more accurate data-driven model, which is not yet reported in other vision-based soft force sensors to the best of our knowledge, achieving state-of-the-art force sensing as shown in Table 1. One can attach the proposed soft networks to almost any rigid grippers, or even soft ones, of compatible sizes to enable high-performing proprioception and omni-directional adaptation simultaneously at a low cost, accomplishing tasks such as sensitive and robust grasping against rigid grippers, impact absorption, and touch-based geometry reconstruction. The contributions of this work are listed as the following:

- Proposed a generic design method for a class of soft polyhedral networks with an embedded vision for proprioception.
- Implemented Sim2Real proprioceptive learning for adaptive kinesthesia to reproduce real-time physical interactions in 3D.
- Proposed visual force learning for viscoelastic proprioception with state-of-the-art 6D force (0.25/0.24/0.35 N) and torque (0.025/0.034/0.006 Nm) sensing.
- Demonstrated competitive capabilities of proprioceptive learning for achieving various fine-motor skills in object handling with robots even after 1 million use cycles.

The rest of this paper is organized as the following. Section 3 introduces the proposed design of the soft finger with omni-directional adaptation and vision-based integration for sensing. Section 4 presents the method of integrating Finite Element Analysis and machine learning to reconstruct the finger’s adaptive kinesthesia in real time for Sim2Real transfer. Section 5 introduces the visual force learning method that leverages the material’s viscoelasticity for static interaction and kinetic motion for dynamic grasping. Section 6 presents experimental results that demonstrate the use of proprioceptive learning for impact absorption and touch-based geometry reconstruction. The conclusion, limitations, and future work are in the final section.

## 2 Related work

### 2.1 Rigid and Soft Finger Adaptation

For industrial scenarios with task-specific needs, robotic fingers or grippers are usually fully actuated with just one or just a few degree-of-freedom (DOFs) with rigid-bodied links or components. Inspired by human fingers, under-actuation

and the integration of softness are widely appreciated when designing robotic fingers that are adaptive to the changes in object geometry [Shimoga and Goldenberg, 1996a,b], where the modeling of contact mechanics and friction limit surfaces enables one to study further the grasping and manipulation problems in robotics [Xydias and Kao, 1999]. Previous work by Hussain et al. [2020] introduced the design method for a tendon-driven, under-actuated gripper with interpenetrating phase composite materials as flexible joints to achieve enhanced adaptation in grasping. Recent development in soft robotics promotes robotic fingers with a full-body soft design that conforms to the object geometry through fluidic actuation and passive adaptation. Recent work by Teeple et al. [2020] presented a soft robotic finger with multi-segmented actuation for enhanced adaptation and dexterity in object manipulation. Further introduction of adaptiveness in the robotic palm is investigated by Subramaniam et al. [2020], where the coupling effects of a soft robotic palm further enhance grasping robustness. Discussion on the softness distribution index by Naselli and Mazzolai [2021] provides a working guideline for designing and modeling soft-bodied robots that are generally applicable to soft continuum manipulators and soft fingers.

The Fin Ray Effect (FRE) soft finger is a design with an excellent adaptation that effectively transforms any industrial gripper into a soft robotic hand. The readers are encouraged to refer to the work by Shan and Birglen [2020] for an in-depth review of the related literature and its theoretical modeling. While the FRE finger can provide geometric adaptation in the 2D plane for grasping, recent work shows a novel finger network design capable of omni-directional adaptation in 3D [Yang et al., 2020], shown as the Pyramid variations in Figure 1A. While equally adaptive to geometric adaptation on the primary interaction face, the finger network design can also produce geometric adaptation from the sideways or on the edge for adaptive grasping [Wan et al., 2020]. It provides a generic design method for a wide range of soft robotic finger networks with similar adaptation in omni-directional interactions [Song and Wan, 2022]. And it also features a hollow volume inside to visually capture its geometric deformation process, which can be integrated with either optical fibers [Yang et al., 2021] or miniature cameras [Wan et al., 2022] for accurate tactile sensing integration. Compared to the FRE finger, the omni-directional adaptation behavior of the omni-finger becomes much more challenging to solve mechanically through analytical modeling, where a data-driven method integrating machine learning [Tapia et al., 2020] and finite element analysis [Duriez, 2013, Largilliere et al., 2015] could be a potential solution.

## 2.2 Sensory Integration during Soft Contact

Scientific literature reports a wide range of sensory integration in robotic manipulation by estimating the soft material’s passive adaptation during contact, including 1) soft fingertips with surface adaptation in the local regions [Lambeta et al., 2020, Shimoga and Goldenberg, 1996a,b] and 2) soft fingers with structural adaptation in the global spaces [Truby et al., 2018, Subramaniam et al., 2020, Teeple et al., 2020]. While both are specifically designed for robotic applications, the artificial skin represents another research stream aiming at a broader range of applications for human-machine interactions [Yan et al., 2021, Zhu et al., 2021]. The *soft robotic fingertip* is widely adopted to capture localized surface deformations during contact. Sensors with one or multiple modalities can be embedded under a small piece of soft material and molded to the size of a fingertip [Wettels et al., 2014, Park et al., 2015]. However, recent research shows a growing adoption of visual sensing by tracking the soft materials’ surface deformation [Yamaguchi and Atkeson, 2016, Yuan et al., 2017]. This strategy significantly reduces design complexity and integration cost while generating a rich perception of contact [Sun et al., 2022]. It should be noted that many soft robotic fingertips are equivalent to artificial skins but with integrated designs packed in a small form factor for convenient installation at the end of existing grippers or fingers.

The *soft robotic finger* represents another approach that involves active or passive actuation of the soft body deformation on a global scale to replace the rigid gripper mechanism for grasping. One could directly integrate artificial skins into robot fingers for the same purpose [Zhu et al., 2021, Heo et al., 2020, Liu et al., 2022]. Many soft robotic fingers leverage both the soft materials’ active and passive deformations and can integrate multiple modalities for tactile sensing [Truby et al., 2018, Kim et al., 2020]. Under fluidic [Terry et al., 2017, Hu and Alici, 2020] or electrical [Li et al., 2019, Acome et al., 2018] actuation, the soft-bodied finger can actively generate geometric deformation to produce a grasping action. During contact, the soft robotic finger can passively conform to the object’s geometry [Cheng et al., 2022, Liu et al., 2021]. Recent work by Wall et al. [2023] shows a sensorization method for soft pneumatic actuators that uses an embedded microphone and speaker to measure different actuator properties. Machine learning algorithms may also be applied to estimate soft body deformations [Hu et al., 2023, Loo et al., 2022, Scharff et al., 2021]. In summary, there remains a challenge in achieving simultaneous contact perception and globalized grasp adaptation at a reduced cost and design complexity for fine motor controls.

Many soft robots are made from polymers such as plastics, rubber, and silica gel [Hu et al., 2023, Cecchini et al., 2023] or metamaterials with structural compliances [Xu et al., 2019, Wan et al., 2022]. Analytical methods using pseudo-rigid-body models (PRBMs) are inherently limited in mechanic assumption to predict the physical interactions

accurately Shan and Birglen [2020]. Viscoelasticity characterizes a time-dependent deformation among soft robots, leading to stress relaxation and creep that are difficult to model [Gutierrez-Lemini, 2013]. In applications where the soft sensor bears dynamic loadings, dynamic hysteresis affects its measurement accuracy [Zou and Gu, 2019, Oliveri et al., 2019]. Difficulties in representing and detecting soft materials’ complex volumetric deformations make it challenging to study viscoelasticity. Many vision-based sensors use a layer of soft skin to isolate the camera from the environment, aiming for stable detection of the interaction physics, such as the intensity of reflective light and marker displacement [Yuan et al., 2017, She et al., 2020]. These sensors mainly capture local deformations on the interaction surfaces. For sensors where the camera is open to the environment, the tracked motions are usually limited to planar movements, and the detection is subject to occlusions [Xu et al., 2021].

### 3 Soft Polyhedral Networks with Embedded Vision for Proprioception

#### 3.1 Soft Polyhedral Networks

A polyhedron is generally understood as a solid geometry in three-dimensional space, featuring polygonal faces connected by straight edges, including prisms, pyramids, and platonic solids [Demaine and O’Rourke, 2007]. Inspired by recent development in soft robotics, we propose a generic design method by turning all edges of a polyhedron into beam structures made from soft materials, then adding layers inside to form a network, followed by redesigning the ends of all mid-layer edges as flexure joints to reduce inferences during deformation while providing sufficient structural support in a compliant manner in Figure 1A. The resultant designs exhibit excellent adaptations in 3D, formulating a class of Soft Polyhedral Networks. This design method is generic, as one can reconfigure the parameters to fine-tune the soft network’s passive adaptation. In this study, we chose the pyramid shape as the base design and modified it with two vertices on top. Figure 1B shows this design features a primary interaction face for typical grasping and a secondary one to enable spatial adaptation, such as 3D twisting. The resultant structure exhibits a large, hollow volume inside with an unobstructed view from the bottom, allowing a direct capture of the adaptive deformations during physical interaction. To attain stable and homogeneous performance, we fabricated the whole network through vacuum molding using polyurethane elastomers (Hei-cast 8400 from H&K) with a mixing ratio of 1:1:0 for its three components to achieve 90A hardness. Alternatively, one can turn to direct 3D printing with TPU or other compliant materials for fabrication [Yi et al., 2019].

#### 3.2 Embedded Motion Tracking

We embedded a miniature motion-tracking system inside the Soft Polyhedral Network to mimic a proprioceptor. As shown in Figure 1C, the system involves a high-speed camera of up to 330 fps (manually adjustable lens, Chengyue WX605 from Weixinshijie) with a large viewing angle ( $170^\circ$ ) fixed on a mounting base inside the network and a plate attached to the network’s first layer with a fiducial marker (ArUco of 16 mm width) stuck to its bottom. The soft network’s spatial adaptation is expressed by its structural compliance, then filtered by the fiducial marker’s spatial movement inside, next captured by the high-speed camera as image features, and finally encoded as a time series of dimensionally reduced 6D pose vector  $\mathbf{D}_t = (D_x, D_y, D_z, D_{rx}, D_{ry}, D_{rz})_t$ , namely, the translation and rotation of the marker relative to its initial pose  $p_0$  before any deformation. The motion tracking system has a high precision of up to 0.005 mm and  $0.018^\circ$ . Table 2 shows that the marker detection has excellent stability at all three resolutions. The system achieves a 100% success detection rate in a test of 8,000 consecutive frames, even at the lowest resolution. In the rest of the paper, we always set the resolution to  $640 \times 360$  at 330 fps.

**Table 2: Tracking stability of the embedded miniature motion capture system.**

Camera Resolution	Distance (mm)	Computation Time (ms)	Range of Fluctuations	
			Positional Noise (mm)	Angular Noise (degree)
640×360	45.6	3.7	[0.014, 0.017, 0.022]	[0.573, 0.514, 0.080]
1280×720	45.2	10.1	[0.015, 0.011, 0.019]	[0.428, 0.214, 0.041]
1920×1080	44.7	16.4	[0.005, 0.009, 0.020]	[0.242, 0.115, 0.018]

We adopt the motion capture solution for its simplicity, transferability, and low cost in mechanical design and algorithmic computation. For example, the motion capture solution can be easily transferred to Soft Polyhedral Networks other than the pyramid shapes, including the prism and platonic ones. One can easily mount the Soft Polyhedral Networks on standard grippers by replacing its current rigid fingertips (Figure 1D). The system proposed in this study involves only three components: the Soft Polyhedral Network, a miniature high-speed camera, and a pair of base frame and mounting

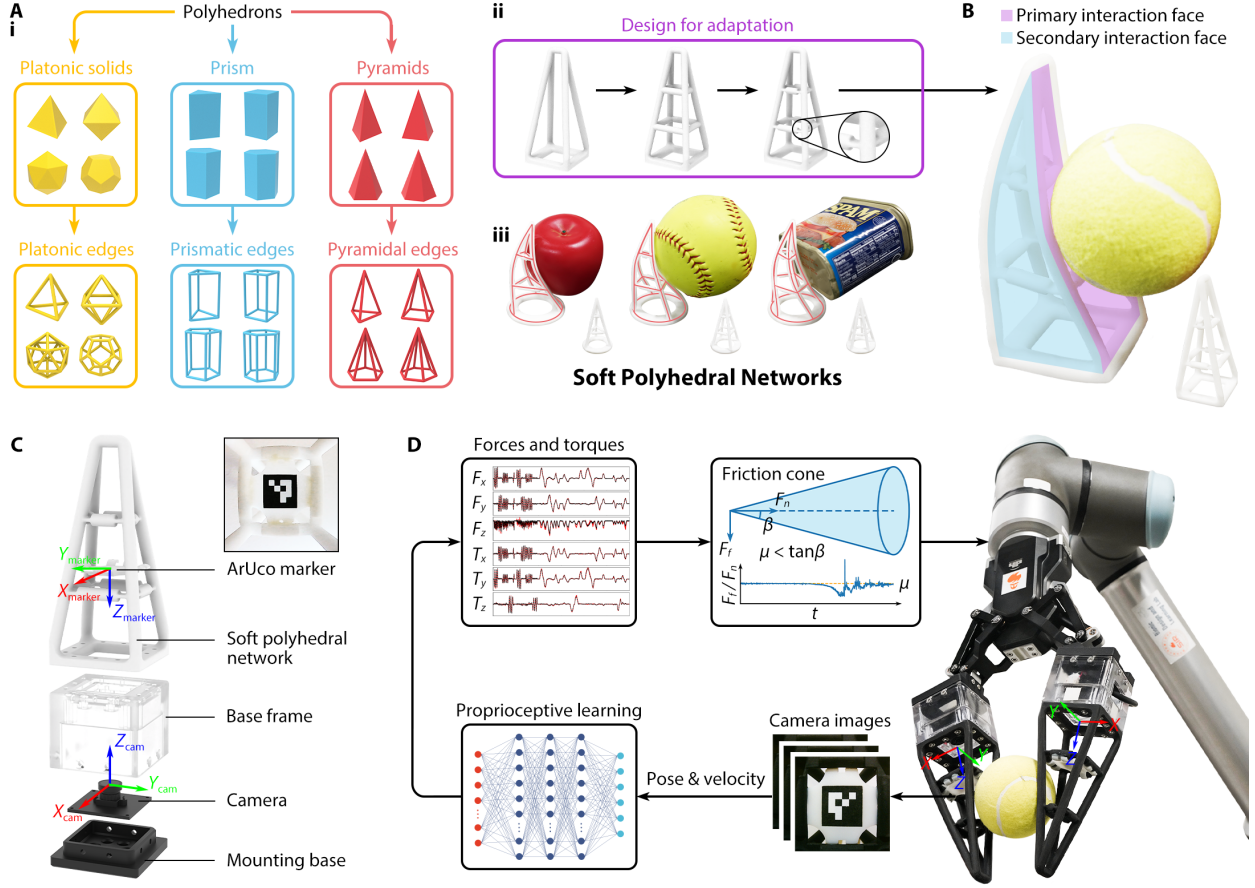


**Figure 1: Soft Polyhedral Network design with embedded vision.** (A) A generic design process applicable to all polyhedrons, (i) starting with removing all faces and replacing all edges with beam structures made from soft materials, then (ii) adding layers inside with the flexure joints, resulting in (iii) a class of soft networks that are geometrically adaptive to external interactions. (B) An enhanced version of the Soft Polyhedral Network with a primary interaction face (marked in pink) and a secondary interaction face (marked in blue). The primary face has an extended contact area with a trapezoid frame, and the secondary face enables adaption in 3D. (C) Exploded view for vision integration by mounting the soft network on top of a base frame housing a high-speed miniature camera, capturing the soft network’s 6D motion during adaptation by tracking an ArUco marker attached inside. (D) The pipeline for proprioceptive learning when using the Soft Polyhedral Network as fingers of a common gripper system. The camera captures the spatial deformation of the soft network by tracking the ArUco marker’s 6D movement. We feed pose and velocity inputs to a neural network to infer 6D forces and torques as the output, which can be further processed to estimate the gripping and shear forces and fed to the robot control loop for reactive object manipulation based on the friction cone model.

base for fixturing. Simplicity in design is the enabling factor of the proposed Soft Polyhedral Network, supporting its robust adaptation with vision-based tactile sensing for robotic manipulation.

## 4 Learning Adaptive Kinesthesia

### 4.1 Stiffness Distribution and FEM Simulation

We conducted a series of unidirectional compression experiments to estimate the stiffness distribution of the Soft Polyhedral Network defined as force over displacement. Figure 2 shows that the soft finger is mounted on a high-performance force/torque sensor (Nano25 from ATI) on top of a custom test rig with two motorized linear motions and two manually driven rotary motions. The force/torque sensor has a resolution of 1/48 N for  $F_x/F_y$ , 1/16 N for  $F_z$ , 0.76 Nmm for  $T_x/T_y$ , and 0.38 Nmm for  $T_z$ . The probe compressed the Soft Polyhedral Network horizontally at 3 mm/s to a pre-defined depth of 15 mm. We conducted the experiments at three different pushing angles ( $\alpha_0$ ,  $\alpha_1$ , and  $\alpha_2$ ),

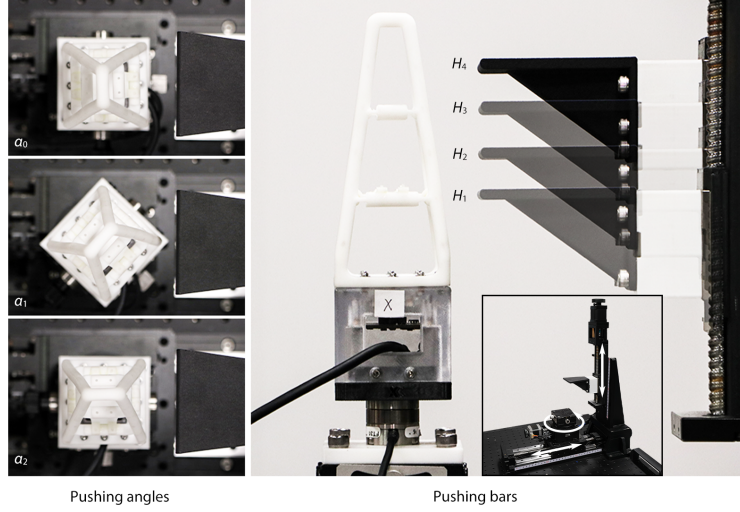


**Figure 2: Experiment setup for measuring stiffness.**

where  $\alpha_0 = 0^\circ$  is to compress the primary interaction face,  $\alpha_1 = 45^\circ$  is to compress the edge between the primary and secondary interaction faces, and  $\alpha_2 = 90^\circ$  is to compress the secondary interaction face. Meanwhile, we also adjust the compression height between  $H_1$  to  $H_4$ . The push displacement  $\delta$  and reaction force  $F$  were recorded to calculate the corresponding stiffness  $k = F/\delta$ .

We used linear elastic elements and non-linear geometry in FEM simulations to model the large adaptive deformation. Calibrated to match the experimental stiffness measurement, the FEM simulation used Young’s modulus of 12.05 MPa, Poisson ratio of 0.5, and density of  $11.3 \text{ g/cm}^3$ , and the solid elements in FEM are 10-node quadratic tetrahedrons with hybrid formulation (C3D10H). The plate for the fiducial marker is a much more rigid body with Young’s modulus of 2,600 MPa. The Soft Polyhedral Network’s bottom is fixed. A total of about 13,000 elements were used in the simulation. The stiffness distribution calculated with simulated data agrees well with the actual measurement in Figure 3, demonstrating a good match between simulation and the soft physical networks. Both measurements share a similar trend where a U-shape stiffness distribution suggests that the primary interaction face is highly adaptive with a conforming geometry during physical interaction. A decreasing stiffness distribution suggests that the edge and secondary interaction face are moderately adaptive. The average absolute error is 0.098 N/mm, and the average relative error is 15.12%. For all experiments, Figure 3 shows a decreasing stiffness distribution along the  $z$ -axis at  $\alpha_1$  and  $\alpha_2$ .

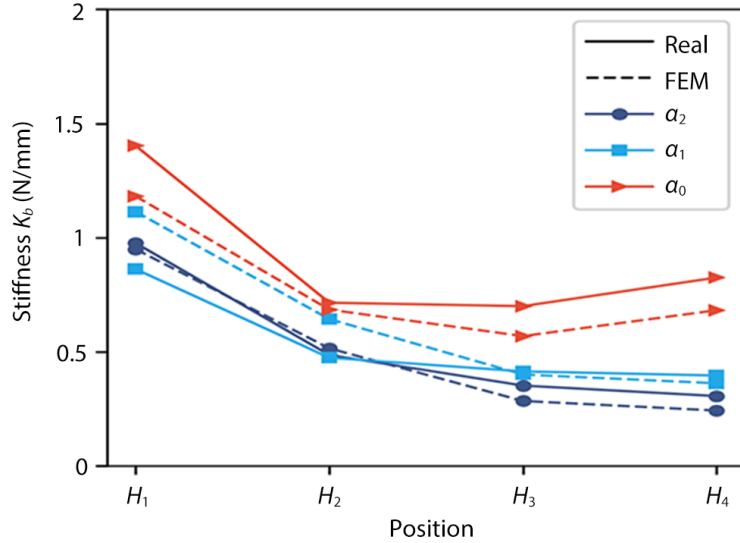


**Figure 3: Stiffness distribution of the Soft Polyhedral Network measured using the test rig and FEM.**

At  $\alpha_0$ , however, the stiffness decreases from 1.4 N/mm at  $H_1$  to a minimum of 0.7 N/mm at  $H_3$ . and increases slightly to 0.825 N/mm at  $H_4$ . This unique stiffness distribution differs from that of the fin ray effect finger, where the stiffness at the fingertip drops to about 25% of the stiffness near the base [Shan and Birglen, 2020].

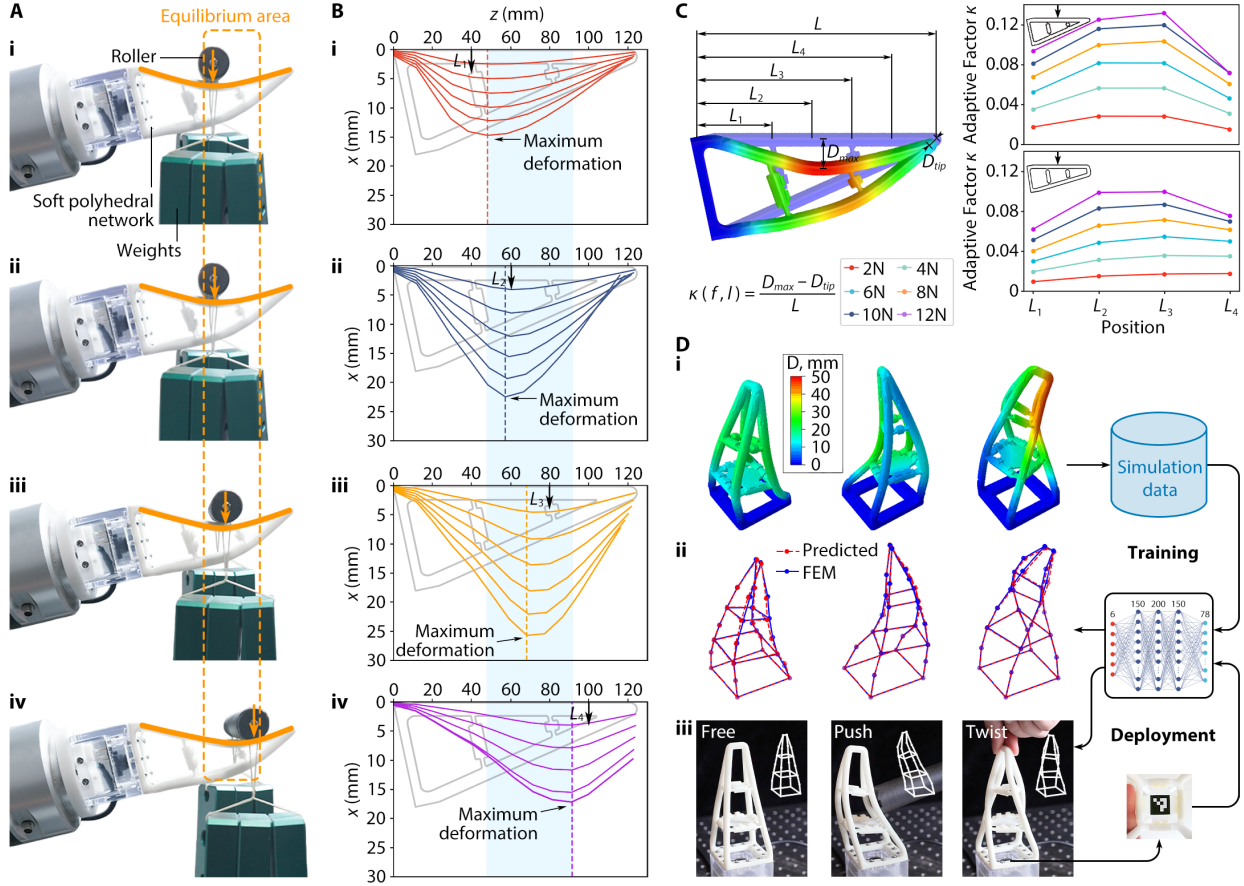


**Figure 4: Learning adaptive kinesthesia with Sim2Real proprioception.** (A) Test for the soft network’s passive adaptation by placing a roller at four different locations (i)~(iv) on the primary interaction face. The roller moves towards an equilibrium area marked in orange dashed lines. (B) FEM simulations of the primary interaction face’s adaptive deformation when applying 2~12 N forces at four initial contact locations marked with arrows. Note that the maximum deformation always occurs within an equilibrium region marked in light blue. (C) Measurement of the adaptive factor  $\kappa$  for the primary and secondary interaction faces. Both faces exhibit passive adaptation with  $\kappa$  maximizing near  $L_3$ , resulting in an enclosed adaptation of the soft network upon external compression. Note that the adaptive capability in the primary interaction face is greater than the secondary one. (D) After (i) collecting FEM simulation data of the soft network under external compressions at various angles and magnitudes, (ii) we train a Sim2Real multi-layer perceptron (MLP) to reproduce the spatial movement of 26 key points on the soft network. (iii) When deployed to the soft network prototype, the MLP predictions align well with observations in free-standing, pushing, and twisting scenarios.

We investigated the soft network’s passive adaptation by placing a 3D-printed roller of 7 mm in diameter with different weights (380~1140 g) at various locations of the primary interaction face along the horizontal direction. Results in Figure 4A show that the roller, supported by a ball bearing on each end, always rolled toward an equilibrium area to a complete stop. During the process, the Soft Polyhedral Network started deforming at the point of contact with a tendency to enclose the roller. This tendency generates an equilibrium area with the highest bending curvature between  $L_2$  and  $L_4$  in Figure 4B, causing the roller to rotate towards the lowest point until an equilibrium state. We studied the same interaction processes by simulation using Finite Element Methods (FEM). Results show that the maximum passive adaptation of the Soft Polyhedral Network always occurs within the shaded area in Figure 4B along the primary interaction face. The resultant spatial compliance is mechanically adaptive to external loadings, which we call “adaptive kinesthesia” of the Soft Polyhedral Network. Here, we define an adaptive factor  $\kappa$  to measure adaptive kinesthesia

under an external force  $f$  exerted at location  $l$  along the primary interaction face  $S_i$  as

$$\kappa_i(f, l) = \frac{D_{max}(l') - D_{tip}}{L}, \quad (1)$$

where  $D_{max}$  is the maximum displacement of the adaptive deformation,  $l'$  is the location of maximum displacement, and  $D_{tip}$  is the tip displacement. The adaptive factor  $\kappa$  reflects how well the network encloses objects along the primary interaction face, with a higher value indicating a better adaption. Figure 4C shows the simulated profiles of adaption for both primary and secondary interaction faces using FEM. All curves share a similar shape, and the adaptive factor  $\kappa$  maximizes near  $L_3$ . We also found that the primary interaction face has better adaptability than the secondary one with  $\kappa_1$  being 1.70, 1.59, 1.48 times  $\kappa_2$  at  $L_1$  to  $L_3$ . The adaptive factor at  $L_4$  was measured at a similar amount (0.94 times), indicating that the segment towards the tip of the network is not as adaptive as the middle but behaves more like a rigid fingernail, which is desirable to produce a firm grasp. The high stiffness at the tip leads to greater adaptive compliance for the pyramid design of the soft network.

## 4.2 Sim2Real Proprioceptive Learning

Kinesthesia is appreciated as the ability to detect active or passive limb movements about a joint, which corresponds to the detection and reproduction of structural movement in the Soft Polyhedral Network during spatial interactions. We propose a Sim2Real learning strategy to detect and reproduce the Soft Polyhedral Network’s adaptive kinesthesia, i.e., the passive proprioception of whole-body movement, using the embedded miniature camera for sensing and FEM data for training. As shown in Figure 4D(i), we collected training data from 12,000 simulations of a soft network model under various loading conditions. The geometry of the simulated soft network is represented by a collection of 26 feature points  $M = \{N_i : (x_i, y_i, z_i) | i = 1, \dots, 26\}$  as shown in Figure 4D(ii), including the intersections of all edges and the mid-points in between. We recorded the coordinates of these feature points and the fiducial marker’s corresponding displacement  $D_t$ . Assuming that the fiducial marker’s spatial movement contains sufficient information to infer the soft network’s adaptive deformation, we trained a regression model based on multi-layer perceptron (MLP) with  $D_t$  as input and the flattened  $M$  as output. The MLP has three hidden layers with 150, 200, and 150 neurons, respectively. The proprioceptive model is evaluated by the positional error  $\sum_{i=1}^{26} \|\hat{N}_i - N_i\|/26$  where  $\hat{N}_i$  is the predicted position of the simulated node  $N_i$  as shown in Figure 5. The average positional error grows as the soft network

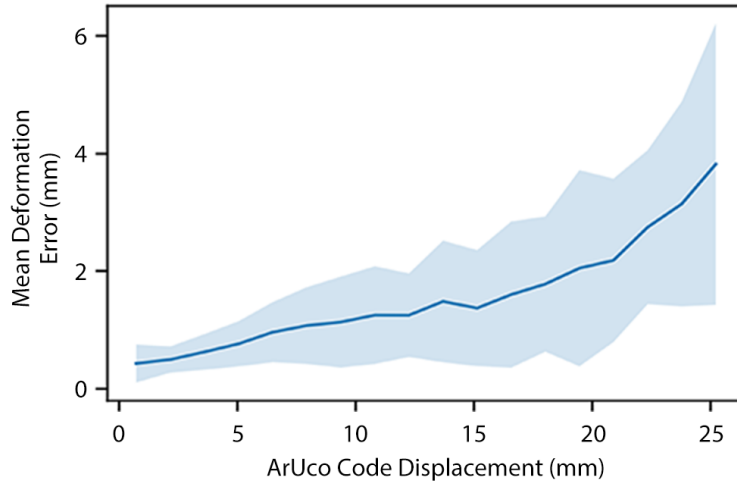


**Figure 5: Mean error distribution of Sim2Real learning for adaptive kinesthesia.** The shaded area indicates one standard deviation of the average positional error.

exhibits large-scale deformations during physical interactions, ranging from 0.4 to less than 4 mm, with an overall average of 1.18 mm. We applied the model trained from simulated data to a real soft network. Each prediction costs 0.4 ms on a laptop with NVIDIA GeForce GTX 1060. We made real-time predictions of its whole-body movement during physical interactions in Figure 4D(iii), demonstrating the power of Sim2Real learning of the soft network’s proprioception in adaptive kinesthesia enhanced by machine learning with FEM (See supplementary material Movie S1).



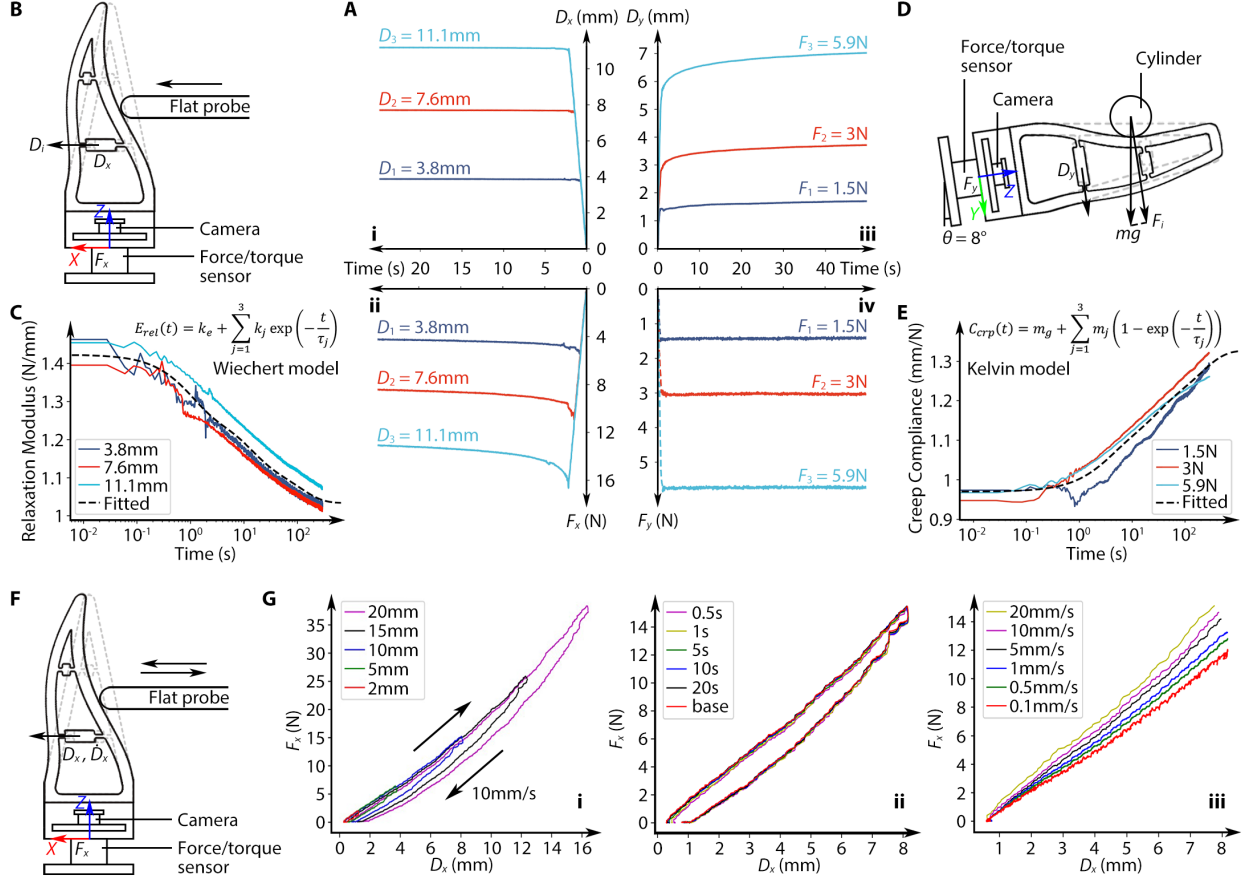


**Figure 6: Viscoelastic analysis of the Soft Polyhedral Network.** (A) Results on the stress relaxation and creep experiments, including i) displacement and ii) force responses by a flat probe along the horizontal direction against the primary interaction face at three fixed distances for relaxation, as well as iii) displacement and iv) force responses by a cylindrical rod along the vertical direction against the secondary interaction face with three different weights for creep. (B) Experiment setup for stress relaxation with a Soft Polyhedral Network fixed vertically on top of a 6-axis FT sensor. (C) Measured relaxation modulus as a function of time and the fitted Wiechert model. (D) Experiment setup for creep test with a Soft Polyhedral Network fixed at  $\gamma = 8^\circ$  to keep the primary interaction face horizontal. (E) Measured creep compliance as a function of time and the fitted Kelvin model. (F) Experiment setup for dynamic loadings against the primary interaction face with a Soft Polyhedral Network fixed vertically on top of a 6-axis FT sensor. (G) Displacement and force responses with a flat probe compressing and de-compressing at different (i) loading depths, (ii) waiting times between cycles, and (iii) speeds.

## 5 Sensing Force and Torque

### 5.1 Viscoelasticity Analysis in Static and Dynamic Interactions

Viscoelasticity describes a material’s characteristic to act like a solid and a fluid, which is universally applicable to robots made from soft matter. The metamaterial design and use of polyurethane for fabrication make the Soft Polyhedral Network responsive to adaptation in a time-dependent and rate-dependent manner. Meanwhile, recent literature suggested including the sense of velocity to extend the concept of proprioception [Ager et al., 2020]. In this section, we report results to characterize the Soft Polyhedral Network’s viscoelastic behaviors in stress relaxation, creep, and dynamic loadings at various interaction speeds.

We started by investigating the Soft Polyhedral Network’s stress relaxation to model its reaction force  $\sigma(t)$  at a longer time scale of  $t$  seconds by applying a constant strain  $\epsilon_0$  at a room temperature of  $25^\circ\text{C}$  [Gutierrez-Lemini, 2013]. We set up the experiment by mounting the soft network on a vibration isolation table with a 6-axis force-torque sensor (Nano25 from ATI) in between, as shown in Figure 6B. A 3D-printed, 5 mm thick, flat probe installed on the tool flange of a robot arm (UR10e from Universal Robots) was used to horizontally compress the soft network’s primary interaction

face at height  $H_2$  to a certain depth  $d$  and held the compression for 300 s. We recorded the marker pose and force/torque readings. Figure 6A(i) shows the soft network's  $x$ -axis displacement over time, where it immediately reaches a stable deformation as the compression completes. Simultaneously, the reaction force  $F_x$  reaches the maximum in Figure 6A(ii), demonstrating the soft network's geometric adaptation during physical interactions. Then,  $F_x$  starts to decrease exponentially until equilibrium. Figure 6C shows the relaxation modulus curves  $E_{rel}(t) = \sigma(t)/\epsilon_0$  at three different depths. We model the stress relaxation process using a Wiechert model, composed of an elastic spring of stiffness  $k_e$  parallel to three Maxwell elements as shown in Figure 7A. Each Maxwell element consists of a Hookean spring of stiffness  $k$  and a Newtonian dashpot of viscosity  $\eta$  connected in series, resulting in a characteristic time  $\tau = \eta/k$ . The fitted Wiechert model is described by

$$E_{rel}(t) = k_e + \sum_{j=1}^3 k_j \exp(-t/\tau_j), \quad (2)$$

where the elastic modulus  $k_e = 1.03$  N/mm, the three Maxwell components  $k_1, k_2, k_3 = 0.15, 0.13, 0.11$  N/mm, and their characteristic relaxation times  $\tau_1, \tau_2, \tau_3 = 1.0, 12.1, 109.5$  s, respectively. Such relaxation response characterizes

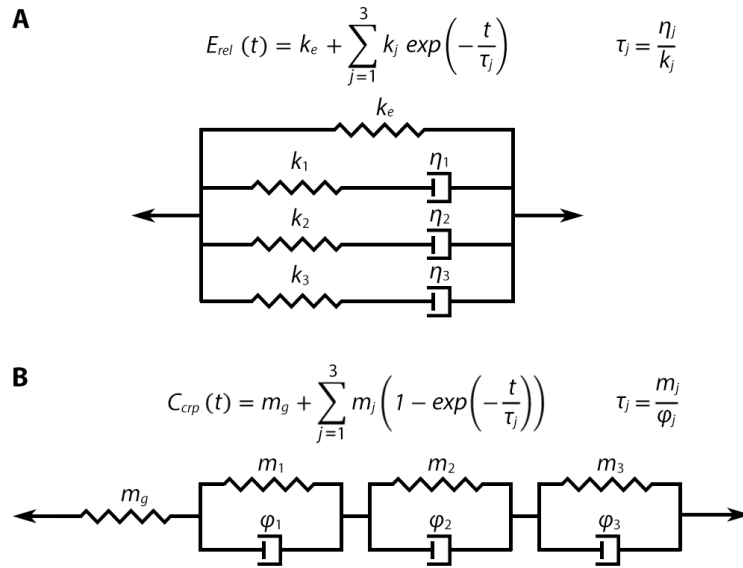


**Figure 7: The Wiechert model for stress relaxation in (A) and the Kelvin model for creep in (B).**

the soft network's viscoelastic behavior, demonstrating adaptations at both geometric and molecular levels. The equilibrium modulus  $E_{rel}(\infty)$  drops by 27% compared to the initial modulus  $E_{rel}(0)$ . This result indicates that for grasping tasks where the fingers must constantly hold the object, especially when the fingers are made from soft materials, the grasp planning algorithm should anticipate a diminishing gripping force due to viscoelastic relaxation to avoid dropping. Current solutions for object manipulation with soft robotic fingers usually adopt an open-loop control to overconstrain the object's movement with form closure [Manti et al., 2015, Zhang et al., 2022]. Our results suggest that further consideration should include viscoelastic relaxation to achieve tactile sensing with fine motor control for object manipulation, especially in scenarios of stress relaxation when the fingers are holding the objects under a fixed position command to close the gripper.

Creep is another phenomenon of viscoelasticity, which measures the time-dependent strain  $\epsilon(t)$  under a constant force  $\sigma_0$  applied on the soft material. The most common scenario is weight compensation while holding an object, which usually occurs on the network's secondary interaction face while holding an object. Using the experimental setup in Figure 6D, we place a cylindrical rod of a 15 mm radius at the center of the network's secondary interaction face. The soft network is tilted at  $\gamma = 8^\circ$  to keep the secondary interaction face horizontal as the contact begins. By attaching different weights to the cylindrical rod, we tested its viscoelastic responses to small, medium, and large static forces of  $F_y$  in 1.5, 3, and 5.9 N. Figure 6A (iii and iv) captures the creep effect with increased marker displacement along the  $y$ -axis. In contrast, the reaction force  $F_y$  immediately reaches a stable state after placing the rod. Figure 6E shows the time-dependent creep compliance curves  $C_{crp}(t) = \epsilon(t)/\sigma_0$ . We model the creep phenomenon using a Kelvin model, composed of a spring of stiffness  $1/m_g$  in series with three Voigt elements as shown in Figure 7B. Each Voigt element consists of a Hookean spring of stiffness  $1/m$  parallel to a Newtonian dashpot of viscosity  $1/\varphi$ , resulting in a

characteristic time  $\tau = m/\varphi$ . The fitted Kelvin model is described by

$$C_{crp}(t) = m_g + \sum_{j=1}^3 m_j [1 - \exp(-t/\tau_j)], \quad (3)$$

where  $t = 0$  s is when external loading is completed, the glassy compliance  $m_g = 0.97$  mm/N, the three Voigt elements  $m_1, m_2, m_3 = 0.10, 0.11, 0.15$  mm/N and the characteristic creep times  $\tau_1, \tau_2, \tau_3 = 3.1, 22.8, 206.2$  s, respectively. The equilibrium compliance  $C_{crp}(\infty)$  increased by a significant 37% compared to the initial compliance  $C_{crp}(0)$ . One can view creep as a reciprocal effect of relaxation. Both characterize the viscoelastic behavior of the network’s molecular adaptation during static interaction. The experimental results agree well with the fact that the relaxation response is faster than creep [Gutierrez-Lemini, 2013].

We also conducted dynamic loading experiments using the setup in Figure 6F to investigate the Soft Polyhedral Network’s nonlinear and viscoelastic behaviors when compressed by a flat probe at different depths, time intervals, and speeds. We recorded the fiducial marker’s  $x$ -axis displacement in cyclic interactions, about 80% of the flat probe’s pushing depth. At an average rate of 10 mm/s, loading and unloading cycles vary at depths between 2 and 20 mm, as shown in Figure 6G(i). The soft network shows non-negligible hysteresis in all experiments. We examined its recovery from deformation by applying consecutive loading and unloading cycles at 10 mm depth with various waiting times ranging from 0.5 to 20 s. As shown in Figure 6G(ii), right after the flat probe disengages with the soft network during unloading, we observe a minor residual strain decreasing rapidly as no further plastic deformation is observable after a waiting time of 5 s. For the two follow-up cycles with a waiting time of 0.5 s, their hysteresis loops almost overlapped even though a residual strain of 0.2 mm existed, demonstrating the soft network’s robust performance against fatigue. To investigate the viscoelasticity of rate dependency, we probed the soft network at different rates ranging from the slowest 0.1 mm/s to the fastest 20 mm/s. Results in Figure 6G(iii) show that the stiffness increases to 25% as the loading rate increases, indicating the non-negligible viscoelastic effects in soft robotic interactions at different speeds.

## 5.2 Visual Force Learning for Viscoelastic Proprioception

Sense of force and effort is another characteristic of proprioception by measuring or reproducing the absolute amount or the relative percentage of force applied. Based on findings on viscoelasticity, we propose a visual force learning method to achieve viscoelastic proprioception by incorporating the Soft Polyhedral Network’s kinetic motions. The overall framework is shown in Figure 8A, where the marker inside the network works like a physical encoder to convert passive, spatial deformations into a 6D pose vector  $\mathbf{D}_t$ , tracked by the miniature motion capture system inside the Soft Polyhedral Network. Then, we developed a decoder model using MLP to infer the corresponding 6D forces and torques ( $F_x, F_y, F_z, T_x, T_y, T_z$ ) as the output. To reflect the speed of interaction during physical contact, we added a velocity term  $\dot{\mathbf{D}}_t = \delta \mathbf{D}_t / \delta t$  to the model input by setting  $\delta t = 15$  ms (or five frames per interval at 330 fps) for more stable tracking.

The simplicity of design enabled us to collect 140,000 samples within 10 minutes by manually interacting with the Soft Polyhedral Network at different heights and speeds. We completed the data collection process within 10 minutes by manually interacting with the Soft Polyhedral Network at different heights ( $H_2$  and  $H_3$ ) and speeds (fast and slow). The collected dataset has 80,000 samples for training and 60,000 for testing, including the frame-by-frame raw images, recognized marker poses, 6D forces and torques from the ATI sensor as the true labels, and the corresponding timestamps. The dataset’s maximum 6D forces and torques are 20 N, 20 N, 10 N, 2 Nm, 2 Nm, and 0.5 Nm, respectively. We normalized inputs and outputs within  $[-1, 1]$  to balance the loss optimization in each dimension for more stable model predictions. The MLP consists of four hidden layers with 1,000, 100, 50, and 6 neurons, respectively (implemented in PyTorch), and were trained with a batch size of 32 using an Adam optimizer with a learning rate of 0.001 on mean squared error loss. We trained the models for 60 epochs and used the one that performed the best on the test dataset.

We trained three models to verify the speed of interactions’ contribution in minimizing the predictions’ mean absolute errors (MAEs) for the 6D force and torque outputs in Figure 8B. When using deformation  $\mathbf{D}_t$  as the only input, the model’s mean absolute errors are 0.51 / 0.46 / 0.43 N ( $F_x/F_y/F_z$ ) in forces and 0.049 / 0.062 / 0.01 Nm ( $T_x/T_y/T_z$ ) in torques. However, after adding deformation rate  $\dot{\mathbf{D}}_t$  to the input features, the prediction errors are reduced by almost half to 0.25 / 0.24 / 0.35 N in forces and 0.025 / 0.034 / 0.006 Nm in torques. The minor improvement in  $F_z$  could be caused by the soft network’s relatively less adaptiveness along the  $z$ -axis by design. Further adding deformation acceleration  $\ddot{\mathbf{D}}_t$  to the input features leads to a slight improvement in performance, suggesting that the  $(\mathbf{D}_t, \dot{\mathbf{D}}_t)$  inputs are sufficiently effective to achieve enhanced visual force learning for viscoelastic proprioception.

We further investigated the hysteresis error of the visual force learning model through comparison against the ground truth using ATI measurements. When using deformation  $\mathbf{D}_t$  as the only input, we observed a hysteresis loop in all predicted force and torque components, as shown in Figure 8C. However, results in Figure 8D show that adding

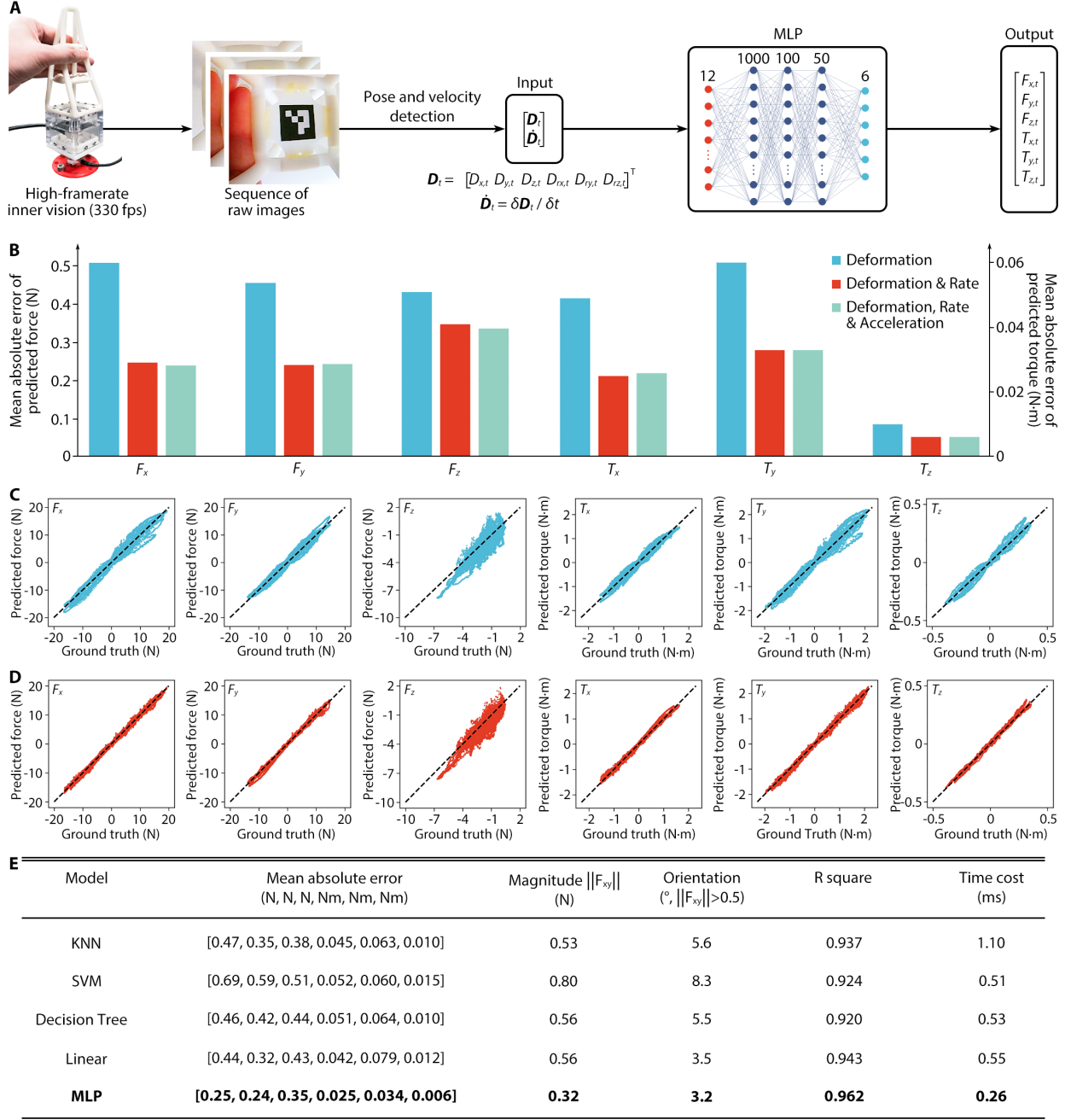


**Figure 8: Visual force learning for viscoelastic proprioception.** (A) The proprioceptive learning pipeline, which starts by image processing for the marker’s pose  $\mathbf{D}_t$  relative to the initial state, then feeds pose  $\mathbf{D}_t$  and its time derivative  $\dot{\mathbf{D}}_t$  to an MLP model to infer 6D forces and torques. (B) The mean absolute errors of the predicted 6D forces and torques using input features including deformation only, deformation & rate, and deformation, rate & acceleration. (C) When trained with the deformation feature only, the forces and torques predicted by the MLP model exhibit observable hysteresis compared to the ground truth. (D) Similar to (C) but trained with deformation and rate as input features, where the hysteresis is largely eliminated. (E) Benchmark when using different models for learning, where the MLP outperformed the rest in all metrics.

deformation rate  $\dot{\mathbf{D}}_t$  to the input features eliminates the hysteresis effects substantially, where the prediction accuracies are consistently stable over different ranges of interactions. The MLP model is computationally efficient, with an average prediction time of 0.26 ms. The chosen camera’s highest fps currently sets the upper bound of the sensing

frequency at 330 Hz, which is still much higher than many existing vision-based tactile sensors from the research literature [Sun et al., 2022, Xu et al., 2021] or commercial products (such as the FT 300 from Robotiq) that run at 100 Hz or less. Higher force-sensing bandwidth is usually preferred for reactive control in real-time physical interactions.

We also benchmarked the MLP with four other models using  $(\mathbf{D}_t, \dot{\mathbf{D}}_t)$  as input, including KNN (K-Nearest-Neighbors), SVM (Support Vector Machine), Decision Tree, and Linear regression. We used the MAEs of forces and torques, the force magnitude accuracy  $\|F_{xy}\|$  and force directional accuracy  $\phi$  of MAEs in the  $x$ - $y$  plane, R-square, and computation time as the evaluation metrics. Results in Figure 8E suggest that the MLP model performs the best in all metrics. The force magnitude and directional accuracies are 0.32 N and 3.2 degrees, respectively. Since the force directional accuracy  $\phi$  is extremely sensitive to disturbances in  $F_x$  or  $F_y$  for samples with small magnitudes, the calculation of directional MAEs only includes examples where force magnitude exceeds 0.5 N. We conducted an ablation study and found that adding kinetic features is crucial in eliminating the hysteresis effect even with linear regressor. At the same time, a more advanced model such as MLP further improves the overall performance.

## 6 Fine-Motor Skills in Object Handling

The overall framework for vision-based proprioceptive learning with the Soft Polyhedral Network proposed in this study consists of three major components, including the Sim2Real learning for kinesthesia adaption, viscoelastic modeling, and visual force learning for viscoelastic proprioception. This section applies the proposed proprioceptive learning with Soft Polyhedral Networks in fine-motor control for object manipulation tasks such as 1) sensitive and competitive grasping and 2) touch-based geometry reconstruction.

### 6.1 Sensitive and Competitive Grasping against Rigid Grippers

We demonstrate the superior performance of the Soft Polyhedral Networks as force-sensitive fingers for rigid grippers. Modern end-effectors, such as the two-finger gripper (Model AG-160-95 by DH-Robotics) shown in Figure 1D, usually come with removable, rigid fingertips that can be easily replaced with the proposed Soft Polyhedral Networks. We fabricated two new prototypes in black color to replace the original rigid fingers of a DH gripper, which was then installed on a collaborative robot (UR10e from Universal Robots) for manipulation tasks in Figure 9. The force/torque sensing model trained from the previous white soft network is directly transferable to the newly fabricated black ones, suggesting the soft networks’ scalability with consistent performances in proprioceptive learning.

In the first experiment, we demonstrate the soft network’s capability in friction estimation during dynamic grasping by gradually closing the fingers while moving upward to pick up a 3D-printed cylinder. Figure 9A shows the two fingers’ coordinate systems. The contact starts at  $t_1$  with an increasing gripping force  $F_g = (F_x^1 + F_x^2) \cos \beta$  detected by the two Soft Polyhedral Networks with different superscripts (Figure 9B). Between  $t_1$  and  $t_2$ , the cylinder did not leave the tabletop, and the soft fingers slid along the cylinder. We estimated the sliding friction’s coefficient  $\mu = F_s/F_g \approx 0.3$ , where the estimated shear force  $F_s = F_y^1 - F_y^2$  equals the sliding friction. At  $t_2$ ,  $F_s$  exceeded the cylinder’s gravity  $G_{cyl}$ , and the sliding friction became static with the cylinder lifted off the table while moving together with the gripper. At  $t_3$ , the gripper stopped closing, and the gripping force reached the maximum. In summary, the Soft Polyhedral Network’s proprioceptive capability was sufficiently accurate to deal with dynamic loadings for friction estimation. However, when the soft gripper is holding the object for a more extended period in Figure 9D, the materials’ stress relaxation causes the actual gripping force  $F'_g$  to drop after  $t_3$  according to  $F'_g(t) = F_g(t_3)E_{rel}(t - t_3)/E_{rel}(0)$  where  $E_{rel}$  is defined in Equation (2) and  $F_g$  is the MLP predicted force. As a result, the ratio  $F_s/F'_g$  increased and approached the friction cone’s boundary, causing the cylinder to tilt with weight imbalance at  $t \approx 14$  s in Figure 9D (See supplementary material Movie S2).

We further demonstrate the soft network’s capability in competitive grasping against rigid grippers and a human finger. The experiment in Figure 9E begins with a Franka Emika holding an orange with its rigid gripper. The gripper with the Soft Polyhedral Networks on a UR10e closes, intending to pull the orange away by moving downward. After contacting the orange at  $t_1$ , the gripper needs to actively adjust its gripping width based on sensory feedback from the Soft Polyhedral Networks in a force control loop to maintain the  $F_s/F_g$  ratio within a predefined friction cone (Figure 9F). Both gripping and shear forces increased simultaneously until the sum of  $F_s$  (4 N) and orange’s gravity  $G_{org}$  exceeded the friction on Franka’s gripper at  $t_2$ , indicating the moment when the orange started to slip from the rigid gripper to the soft fingers. Then, the shear force decreased and changed direction to counteract the orange’s weight while the orange was fully secured within the soft fingers at  $t_3$  (See supplementary material Movie S3). We also conduct a follow-up experiment in Figure 9G by manually pushing the orange out of the soft fingers. Results in Figure 9H demonstrate the Soft Polyhedral Networks’ dynamic capability in proprioceptive learning to retain the orange from four attempts by the human finger with a maximum gripping force of 18 N.

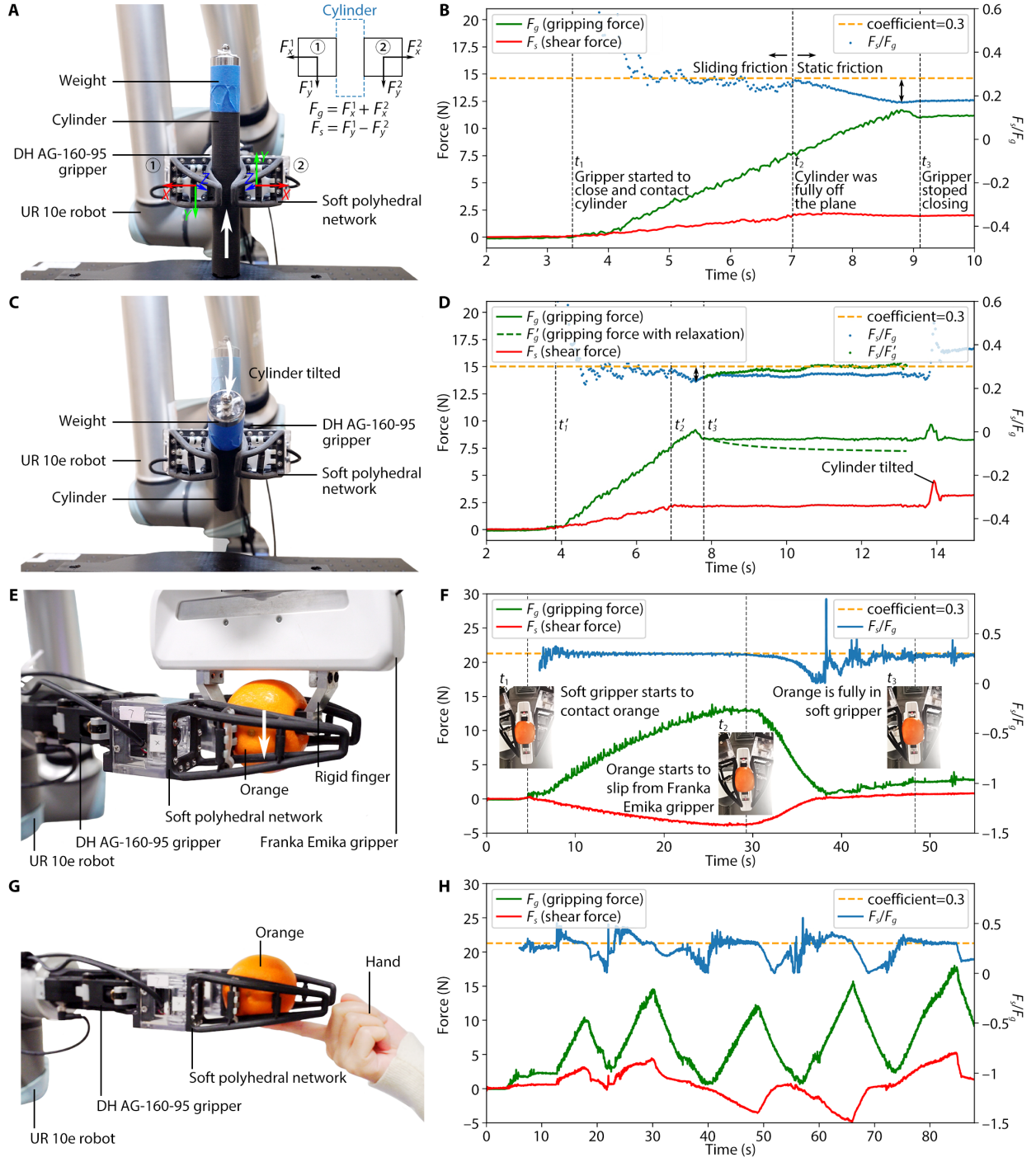


**Figure 9: Sensitive and robust grasping of the Soft Polyhedral Networks as robotic fingers.** (A) Setup for a cylinder grasping task by replacing the gripper’s original rigid fingertips with Soft Polyhedral Networks. (B) The measured gripping and shear forces, where the coefficient of sliding friction  $\mu$  is estimated by  $F_s/F_g$ . The gripper produces enough friction against the cylinder’s gravity to lift it off the table. (C)~(D) The same cylinder grasping task but with a gripping force approaching the frictional cone’s boundary. The cylinder is lifted initially but tilts because the gripping force decreases due to viscoelastic relaxation and exceeds the friction cone. (E)~(F) Setup and results of an orange grasping task completed in a force control loop by maintaining the gripping and shear forces within a predefined friction cone, where the soft fingers successfully grabbed the orange from the rigid fingers. (G)~(H) Setup and results for an orange grasping task against disturbance from a human hand, where the soft fingers protect the orange from pushing attempts made by the human fingers.

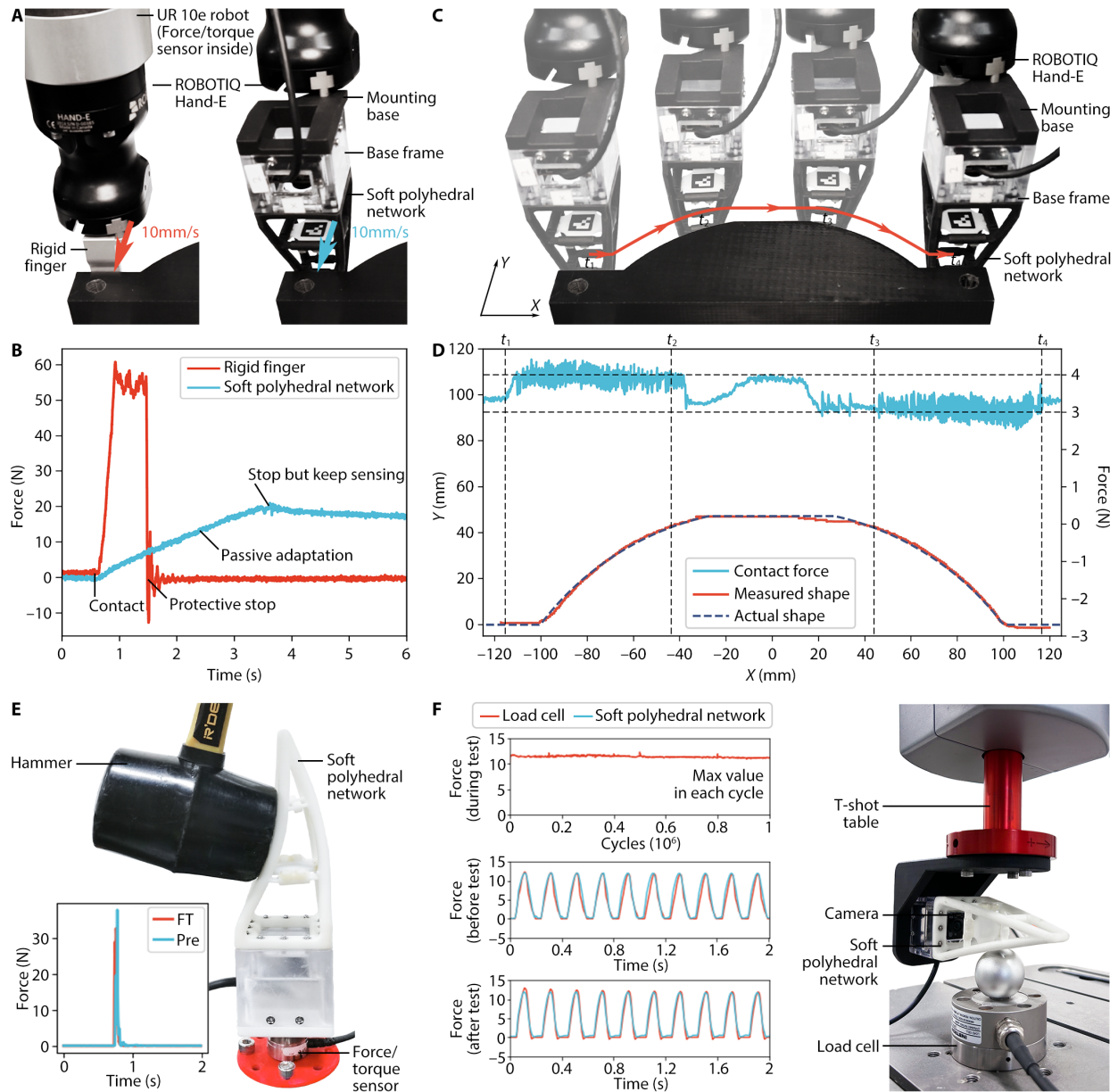


**Figure 10: Tactile reconstruction and impact absorption of the Soft Polyhedral Network.** (A) Setup for impact absorption comparison between the original rigid finger and a Soft Polyhedral Network as the finger when the fingers hit a rigid obstacle at 10 mm/s. (B) The rigid collision generates a 60 N impact force that instantly triggers a protective stop in the robot controller, whereas the soft collision only generates 20 N within 3 s. (C) Setup for touch-base geometry reconstruction using the soft network as the finger by sliding along the arch contour of a 3D-printed object by maintaining the contact force  $F_{xy}$  between 3 to 4 N. (D) Experiment results of the reconstruction by touch indicating the contact force in light blue lines, and the gripper trajectory as the reproduced geometry in red lines. (E) When hit by a hammer, the soft network remains functional while accurately measuring the impact force. (F) Setup and results for fatigue test. The soft network moved downward at a frequency of 5 Hz for one million cycles and maintained stable mechanical properties and proprioceptive prediction ability.

## 6.2 Impact Absorption and Touch-based Geometry Reconstruction

The Soft Polyhedral Network’s proprioceptive capability can also sense and absorb impacts during a collision, supporting continuous task completion without interruption, representing a practical demand from modern production lines with robots (See supplementary material Movie S4). For a collaborative robot (UR10e from Universal Robots) with rigid fingers on its gripper (Hand-E from Robotiq) in Figure 10A,

a collision of 10 mm/s incurs an impact force up to 60 N for nearly 1 s, measured by the F/T sensor inside the flange until the protective stop is triggered in the controller in Figure 10B. However, after replacing the rigid fingertip with the soft network, the measured impact was much reduced to one-third the amount (20 N) within three times the duration, resulting in a combined 9X improvement in safety factor. The soft network’s passive deformation effectively absorbed the impact without causing an emergency stop, enabling the system to continue with predefined tasks, such as the tactile reconstruction task shown in Figure 10C. In this experiment, we implemented a force control strategy by keeping the contact force between the soft network and the arch shape workpiece between 3 and 4 N in the  $x$ - $y$  plane, letting the soft network slide along the target object’s contour for geometry reconstruction. Figure 10D shows that the recorded trajectory skillfully reconstructs the target object’s geometry.

We also tested the robustness and durability of the Soft Polyhedral Network’s proprioceptive prediction under sudden or repetitive impacts. In Figure 10E, we struck the primary interaction surface using a hammer while mounting the network on top of an F/T sensor (Nano25 from ATI) on a table. The F/T sensor detected a sudden impact up to 35 N within 34 ms, and the predicted result matched the sensor readings with a robust performance. In Figure 10F, we performed a fatigue test for the Soft Polyhedral Network on the Instron® ElectroPuls® E3000. The soft network was mounted on the T-shot table and moved cyclically downward at a frequency of 5 Hz, with a maximum displacement of 10 mm and a resultant force of 13 N. The soft network contacted the rigid ball fixed on the load cell, causing its deformation. During the one-million-cycle loading process, the contact forces recorded by the load cell remained between 11.0 and 11.8 N, demonstrating that the network maintained stable mechanical properties (See supplementary material Movie S5). In addition, the soft network’s predicted forces agree well with the forces recorded by the load cell before and after one million loading cycles, proving that the fingers had robust and durable proprioceptive prediction ability.

## 7 Conclusion, Limitation, and Future Work

The medical literature often regards proprioception as the sixth sense that tells us what the body itself is doing. It involves the sense of position and movement and the sense of force and effort through our musculoskeletal system, a skill essential for the robot to acquire for intelligent interaction with the physical world. During the moment of touch, the sensing receptors under our skin detect the object’s physical properties through a mixture of modalities and simultaneously react by adjusting the muscle contraction with skeletal movement to facilitate a natural interaction from within. In comparison, classical design methods through rigid-body mechanics excel in accuracy and speed, and emerging solutions in soft robotics support an overconstrained interaction through under-actuated designs that are passively adaptive to the unstructured environment with mechanical intelligence. In this study, we proposed the design of a class of Soft Polyhedral Networks capable of whole-body compliance adaptive to external interactions with an embedded vision-based motion capture system inside. We achieved adaptive kinesthesia using Sim2Real learning from FEM data to reproduce the soft network’s whole-body position and movement during passive adaptation in real-time. We also proposed a visual force learning method for viscoelastic proprioception by adding velocity terms to the positional input features to infer more accurate senses of force and effort using neural networks. The prototypes presented in this study use only one off-the-shelf camera board with two 3D-printed components while being functionally compliant in 3D with sensory feedback in 6D, much cheaper than commercial 6-axis force-torque sensors to facilitate mass adoption. Within a compact form factor and a wide range of design variations, one can easily customize the Soft Polyhedral Network to suit the changing needs for force-controllable interactions in modern robotics with transferable, robust, real-time proprioceptive learning.

The polyhedron-inspired network design proposed in this work is a versatile method to introduce customizable spatial compliance to physical interactions in robotics with ample design space for further optimization. We selected a particular design in this study with enhanced performance for grasping, featuring a primary interaction face with a larger contact area for adaptive grasping and a secondary one to facilitate spatial compliance. One can degenerate the design to 2D compliance by changing the soft network into a multi-layered structure, resulting in a design like Festo’s Fin-ray finger. Such degenerated 2D structure is limited to purely planar adaptation only with an obstructed interior view, challenging for vision integration in applications [Xu et al., 2021]. The polyhedron-inspired geometry greatly enhanced the design variations while enabling spatial adaptation to preserve the proprioceptive learning capability with sense. We can also add layers of friction-resistive material [Li et al., 2022b, 2020] or introduce bio-inspired texture [Zhang et al., 2020] directly on the primary interaction face to further enhance the Soft Polyhedral Network’s performances in grasping.



One can also modify the design to make the beams hollow, allowing fluidic actuation to adjust the stiffness distribution of the whole network to maximize the power of soft robotics, but at the cost of added complexities in pressurized fluidic power source and system design.

The Soft Polyhedral Network is simple, accurate, and robust in producing stable mechanical properties and proprioceptive predictions even after one million compression cycles, accommodating physical interactions for robotic manipulation in tasks such as sensitive and competitive grasping and touch-based geometry reconstruction. Considering the low cost of the material and parts and the relatively large load of each push presented in the experiments, our design is remarkably durable. It is worth noting that only the soft network part needs replacement during maintenance, while the camera base and learning algorithms can be reused. The off-the-shelf camera board currently limits the size, frequency, and processing power of the Soft Polyhedral Network. With added cost in custom development, we can further upgrade the camera with a higher framerate in a smaller size, use battery-powered onboard processing for edge computing and wireless communication, and introduce active lighting with LEDs for a more stable capture of image features. We also point out that the pyramid design used in this study is limited in adaptation along the  $z$ -axis, mainly chosen with an enhanced adaptation in the  $x$ - $y$  plane for grasping, resulting in a less accurate force estimation along the  $z$ -axis. This issue can be addressed using different network designs for passive adaptation in desirable axes.

The simplicity of the Soft Polyhedral Network design strengthens the integration of visual features to support learning-based capabilities in a more challenging environment. For example, with simple waterproofing of the base mount and the camera inside, the system can be directly used underwater while maintaining proprioception. One can obliterate the marker by processing full images of the soft network deformations with advanced neural networks, such as variational auto-encoders, for proprioceptive learning but at the cost of explainability, transferability, and accuracy. Recent advances in generative models could also be a promising solution to automatically remove the network in the image with generated pixels of the physical world so that the camera can be alternatively used as a vision sensor for object detection. Investigations into the viscoelastic behaviors of the Soft Polyhedral Networks demonstrate the importance of including kinetic features while integrating machine learning with soft robots. We can use a single high-framerate vision sensor to capture the soft network’s dynamic physical interaction process with a rich collection of visual features to support a learning-based approach. With the vision-based solution and learning algorithms, if relaxing the need for functional passive adaptation, one can use almost any deformable, hollow structure on top of the camera to achieve proprioceptive learning presented in this work, as long as a reasonable volume inside is within the camera’s viewing angles during physical interactions.

## Acknowledgements

This work is partly funded by the National Natural Science Foundation of China under Grant 62206119, the Science, Technology, and Innovation Commission of Shenzhen Municipality under Grants ZDSYS20220527171403009 and JCYJ20220818100417038, and Guangdong Provincial Key Laboratory of Human-Augmentation and Rehabilitation Robotics in Universities.

## Supporting Videos

- Movie S1. Sim2Real proprioception for adaptive kinesthesia.
- Movie S2. Viscoelastic sensitive grasping for friction estimation.
- Movie S3. Competitive grasping for an orange.
- Movie S4. Impact absorption and tactile reconstruction using visual force learning.
- Movie S5. Million cycle fatigue test.

## References

- JL Taylor. *Proprioception*, pages 1143–1149. Oxford: Academic Press, 2009. ISBN 978-0-08-045046-9.
- Insang You, David G Mackanic, Naoji Matsuhisa, Jiheong Kang, Jimin Kwon, Levent Beker, Jaewan Mun, Wonjeong Suh, Tae Yeong Kim, Jeffrey B-H Tok, et al. Artificial multimodal receptors based on ion relaxation dynamics. *Science*, 370(6519):961–965, 2020.
- Guozhen Li, Shiqiang Liu, Qian Mao, and Rong Zhu. Multifunctional electronic skins enable robots to safely and dexterously interact with human. *Advanced Science*, 9(11):2104969, 2022a.
- Ming Wang, Yifei Luo, Ting Wang, Changjin Wan, Liang Pan, Shaowu Pan, Ke He, Aden Neo, and Xiaodong Chen. Artificial skin perception. *Advanced Materials*, 33(19):2003014, 2021.

- Kiju Lee, Yanzhou Wang, and Chuanqi Zheng. TWISTER hand: Underactuated robotic gripper inspired by origami twisted tower. *IEEE Transactions on Robotics*, 36(2):488–500, 2020.
- Lael U. Odhner, Leif P. Jentoft, Mark R. Claffee, Nicholas Corson, Yaroslav Tenzer, Raymond R. Ma, Martin Buehler, Robert Kohout, Robert D. Howe, and Aaron M. Dollar. A compliant, underactuated hand for robust manipulation. *The International Journal of Robotics Research*, 33(5):736–752, 2014.
- Yin Zhang, Wang Zhang, Pan Gao, Xiaoqing Zhong, and Wei Pu. Finger-palm synergistic soft gripper for dynamic capture via energy harvesting and dissipation. *Nature Communications*, 13(1):7700, 2022.
- Zhongda Sun, Minglu Zhu, Zixuan Zhang, Zhaocong Chen, Qiongfeng Shi, Xuechuan Shan, Raye Chen Hua Yeow, and Chengkuo Lee. Artificial intelligence of things (aiot) enabled virtual shop applications using self-powered sensor enhanced soft robotic manipulator. *Advanced Science*, 8(14):2100230, 2021.
- Hamed Joodaki and Matthew B Panzer. Skin mechanical properties and modeling: A review. *Proceedings of the Institution of Mechanical Engineers, Part H: Journal of Engineering in Medicine*, 232(4):323–343, 2018.
- Cameron H. Parvini, Alexander X. Cartagena-Rivera, and Santiago D. Solares. Viscoelastic parameterization of human skin cells characterize material behavior at multiple timescales. *Communications Biology*, 5(1):17, 2022.
- Deepika Malhotra, Sharadwata Pan, Lars R  ther, Thomas B. Goudoulas, Gerrit Schlippe, Werner Voss, and Natalie Germann. Linear viscoelastic and microstructural properties of native male human skin and in vitro 3d reconstructed skin models. *Journal of the Mechanical Behavior of Biomedical Materials*, 90:644–654, 2019.
- Qi Wang and Vincent Hayward. In vivo biomechanics of the fingerpad skin under local tangential traction. *Journal of Biomechanics*, 40(4):851–860, 2007.
- Fang Wan, Xiaobo Liu, Ning Guo, Xudong Han, Feng Tian, and Chaoyang Song. Visual Learning towards Soft Robot Force Control using a 3D Metamaterial with Differential Stiffness. In Aleksandra Faust, David Hsu, and Gerhard Neumann, editors, *Conference on Robot Learning (CoRL)*, volume 164 of *Proceedings of Machine Learning Research*, pages 1269–1278. PMLR, 08–11 Nov 2022.
- Wenzhen Yuan, Siyuan Dong, and Edward H. Adelson. GelSight: High-resolution robot tactile sensors for estimating geometry and force. *Sensors*, 17(12), 2017.
- Huanbo Sun, Katherine J. Kuchenbecker, and Georg Martius. A soft thumb-sized vision-based sensor with accurate all-round force perception. *Nature Machine Intelligence*, 4(2):135–145, 2022.
- Thomas George Thuruthel, Benjamin Shih, Cecilia Laschi, and Michael Thomas Tolley. Soft robot perception using embedded soft sensors and recurrent neural networks. *Science Robotics*, 4(26):eaav1488, 2019.
- Xiaowei Shan and Lionel Birglen. Modeling and analysis of soft robotic fingers using the fin ray effect. *The International Journal of Robotics Research*, 39(14):1686–1705, 2020.
- Wenfu Xu, Heng Zhang, Han Yuan, and Bin Liang. A compliant adaptive gripper and its intrinsic force sensing method. *IEEE Transactions on Robotics*, 37(5):1584–1603, 2021.
- K.B. Shimoga and A.A. Goldenberg. Soft robotic fingertips: Part i: A comparison of construction materials. *The International Journal of Robotics Research*, 15(4):320–334, 1996a.
- K.B. Shimoga and A.A. Goldenberg. Soft robotic fingertips: Part ii: Modeling and impedance regulation. *The International Journal of Robotics Research*, 15(4):335–350, 1996b.
- Nicholas Xydias and Imin Kao. Modeling of contact mechanics and friction limit surfaces for soft fingers in robotics, with experimental results. *The International Journal of Robotics Research*, 18(9):941–950, 1999.
- Irfan Hussain, Oraib Al-Ketan, Federico Renda, Monica Malvezzi, Domenico Prattichizzo, Lakmal Seneviratne, Rashid K Abu Al-Rub, and Dongming Gan. Design and prototyping soft–rigid tendon-driven modular grippers using interpenetrating phase composites materials. *The International Journal of Robotics Research*, 39(14):1635–1646, 2020.
- Clark B Teeple, Theodore N Koutros, Moritz A Graule, and Robert J. Wood. Multi-segment soft robotic fingers enable robust precision grasping. *The International Journal of Robotics Research*, 39(14):1647–1667, 2020.
- Vignesh Subramaniam, Snehal Jain, Jai Agarwal, and Pablo Valdivia y Alvarado. Design and characterization of a hybrid soft gripper with active palm pose control. *The International Journal of Robotics Research*, 39(14):1668–1685, 2020.
- Giovanna A Naselli and Barbara Mazzolai. The softness distribution index: towards the creation of guidelines for the modeling of soft-bodied robots. *The International Journal of Robotics Research*, 40(1):197–223, 2021.
- Linhan Yang, Fang Wan, Haokun Wang, Xiaobo Liu, Yujia Liu, Jia Pan, and Chaoyang Song. Rigid-soft interactive learning for robust grasping. *IEEE Robotics and Automation Letters*, 5(2):1720–1727, 2020.

- Fang Wan, Haokun Wang, Jiyuan Wu, Yujia Liu, Sheng Ge, and Chaoyang Song. A reconfigurable design for omni-adaptive grasp learning. *IEEE Robotics and Automation Letters*, 5(3):4210–4217, 2020.
- Chaoyang Song and Fang Wan. Robotic network structure and sensing system suitable for unstructured environment (us patent us20220147052), 2022.
- Linhan Yang, Xudong Han, Weijie Guo, Fang Wan, Jia Pan, and Chaoyang Song. Learning-based optoelectronically innervated tactile finger for rigid-soft interactive grasping. *IEEE Robotics and Automation Letters*, 6(2):3817–3824, 2021.
- Javier Tapia, Espen Knoop, Mojmir Mutný, Miguel A. Otaduy, and Moritz Bächer. Makesense: Automated sensor design for proprioceptive soft robots. *Soft Robotics*, 7(3):332–345, 2020.
- Christian Duriez. Control of elastic soft robots based on real-time finite element method. In *IEEE International Conference on Robotics and Automation (ICRA)*, pages 3982–3987, 2013.
- Frederick Largilliere, Valerian Verona, Eulalie Coevoet, Mario Sanz-Lopez, Jeremie Dequidt, and Christian Duriez. Real-time control of soft-robots using asynchronous finite element modeling. In *IEEE International Conference on Robotics and Automation (ICRA)*, pages 2550–2555, 2015.
- Mike Lambeta, Po-Wei Chou, Stephen Tian, Brian Yang, Benjamin Maloon, Victoria Rose Most, Dave Stroud, Raymond Santos, Ahmad Byagowi, Gregg Kammerer, Dinesh Jayaraman, and Roberto Calandra. DIGIT: A novel design for a low-cost compact high-resolution tactile sensor with application to in-hand manipulation. *IEEE Robotics and Automation Letters*, 5(3):3838–3845, 2020.
- Ryan L. Truby, Michael Wehner, Abigail K. Grosskopf, Daniel M. Vogt, Sebastien G. M. Uzel, Robert J. Wood, and Jennifer A. Lewis. Soft somatosensitive actuators via embedded 3d printing. *Advanced Materials*, 30(15):1706383, 2018.
- Youcan Yan, Zhe Hu, Zhengbao Yang, Wenzhen Yuan, Chaoyang Song, Jia Pan, and Yajing Shen. Soft magnetic skin for super-resolution tactile sensing with force self-decoupling. *Science Robotics*, 6(51):eabc8801, 2021.
- Pang Zhu, Huifeng Du, Xingyu Hou, Peng Lu, Liu Wang, Jun Huang, Ningning Bai, Zhigang Wu, Nicholas X. Fang, and Chuan Fei Guo. Skin-electrode iontronic interface for mechanosensing. *Nature Communications*, 12(1):4731, 2021.
- Nicholas Wettels, Jeremy A. Fishel, and Gerald E. Loeb. *Multimodal Tactile Sensor*, pages 405–429. Springer International Publishing, Cham, 2014. ISBN 978-3-319-03017-3.
- Jonghwa Park, Marie Kim, Youngoh Lee, Heon Sang Lee, and Hyunhyub Ko. Fingertip skin-inspired microstructured ferroelectric skins discriminate static/dynamic pressure and temperature stimuli. *Science Advances*, 1(9):e1500661, 2015.
- Akihiko Yamaguchi and Christopher G. Atkeson. Combining finger vision and optical tactile sensing: Reducing and handling errors while cutting vegetables. In *IEEE-RAS International Conference on Humanoid Robots (Humanoids)*, pages 1045–1051, 2016.
- Si-Hwan Heo, Cheolgyu Kim, Taek-Soo Kim, and Hyung-Soon Park. Human-palm-inspired artificial skin material enhances operational functionality of hand manipulation. *Advanced Functional Materials*, 30(25):2002360, 2020.
- Mengwei Liu, Yujia Zhang, Jiachuang Wang, Nan Qin, Heng Yang, Ke Sun, Jie Hao, Lin Shu, Jiarui Liu, Qiang Chen, Pingping Zhang, and Tiger H. Tao. A star-nose-like tactile-olfactory bionic sensing array for robust object recognition in non-visual environments. *Nature Communications*, 13(1):79, 2022.
- Sang Yup Kim, Youngwoo Choo, R. Adam Bilodeau, Michelle C. Yuen, Gilad Kaufman, Dylan S. Shah, Chinedum O. Osuji, and Rebecca Kramer-Bottiglio. Sustainable manufacturing of sensors onto soft systems using self-coagulating conductive pickering emulsions. *Science Robotics*, 5(39):eaay3604, 2020.
- Seppe Terryn, Joost Brancart, Dirk Lefeber, Guy Van Assche, and Bram Vanderborght. Self-healing soft pneumatic robots. *Science Robotics*, 2(9):eaan4268, 2017.
- Weiping Hu and Gursel Alici. Bioinspired three-dimensional-printed helical soft pneumatic actuators and their characterization. *Soft Robotics*, 7(3):267–282, 2020.
- Jinrong Li, Liwu Liu, Yanju Liu, and Jinsong Leng. Dielectric elastomer spring-roll bending actuators: Applications in soft robotics and design. *Soft Robotics*, 6(1):69–81, 2019.
- E. Acome, S. K. Mitchell, T. G. Morrissey, M. B. Emmett, C. Benjamin, M. King, M. Radakovitz, and C. Keplinger. Hydraulically amplified self-healing electrostatic actuators with muscle-like performance. *Science*, 359(6371):61–65, 2018.

- Jianxiang Cheng, Rong Wang, Zechu Sun, Qingjiang Liu, Xiangnan He, Honggeng Li, Haitao Ye, Xingxin Yang, Xinfeng Wei, Zhenqing Li, Bingcong Jian, Weiwei Deng, and Qi Ge. Centrifugal multimaterial 3d printing of multifunctional heterogeneous objects. *Nature Communications*, 13(1):7931, 2022.
- Shoufeng Liu, Fujun Wang, Zhu Liu, Wei Zhang, Yanling Tian, and Dawei Zhang. A two-finger soft-robotic gripper with enveloping and pinching grasping modes. *IEEE/ASME Transactions on Mechatronics*, 26(1):146–155, 2021.
- Vincent Wall, Gabriel Zöllner, and Oliver Brock. Passive and active acoustic sensing for soft pneumatic actuators. *The International Journal of Robotics Research*, 42(3):108–122, 2023.
- Delin Hu, Francesco Giorgio-Serchi, Shiming Zhang, and Yunjie Yang. Stretchable e-skin and transformer enable high-resolution morphological reconstruction for soft robots. *Nature Machine Intelligence*, 5(3):261–272, 2023.
- Junn Yong Loo, Ze Yang Ding, Vishnu Monn Baskaran, Surya Girinatha Nurzaman, and Chee Pin Tan. Robust multimodal indirect sensing for soft robots via neural network-aided filter-based estimation. *Soft Robotics*, 9(3): 591–612, 2022.
- Rob B. N. Scharff, Guoxin Fang, Yingjun Tian, Jun Wu, Jo M. P. Geraedts, and Charlie C.L. Wang. Sensing and reconstruction of 3-d deformation on pneumatic soft robots. *IEEE/ASME Transactions on Mechatronics*, 26(4): 1877–1885, 2021.
- Luca Cecchini, Stefano Mariani, Marilena Ronzan, Alessio Mondini, Nicola M. Pugno, and Barbara Mazzolai. 4d printing of humidity-driven seed inspired soft robots. *Advanced Science*, 10(9):2205146, 2023.
- Patricia A Xu, Anand Kumar Mishra, Hedan Bai, Cameron A Aubin, Letizia Zullo, and Robert F Shepherd. Optical lace for synthetic afferent neural networks. *Science robotics*, 4(34):eaaw6304, 2019.
- Danton Gutierrez-Lemini. *Engineering Viscoelasticity*. Springer New York, NY, 2013.
- Jiang Zou and Guoying Gu. High-precision tracking control of a soft dielectric elastomer actuator with inverse viscoelastic hysteresis compensation. *IEEE/ASME Transactions on Mechatronics*, 24(1):36–44, 2019.
- Alberto Oliveri, Martina Maselli, Matteo Lodi, Marco Storace, and Matteo Cianchetti. Model-based compensation of rate-dependent hysteresis in a piezoresistive strain sensor. *IEEE Transactions on Industrial Electronics*, 66(10): 8205–8213, 2019.
- Yu She, Sandra Q. Liu, Peiyu Yu, and Edward Adelson. Exoskeleton-covered soft finger with vision-based proprioception and tactile sensing. In *IEEE International Conference on Robotics and Automation (ICRA)*, pages 10075–10081, 2020.
- Erik D Demaine and Joseph O’Rourke. *Geometric Folding Algorithms: Linkages, Origami, Polyhedra*. Cambridge university press, 2007.
- Juan Yi, Xiaojiao Chen, Chaoyang Song, Jianshu Zhou, Yujia Liu, Sicong Liu, and Zheng Wang. Customizable three-dimensional-printed origami soft robotic joint with effective behavior shaping for safe interactions. *IEEE Transactions on Robotics*, 35(1):114–123, 2019.
- Amanda L. Ager, Dorien Borms, Lode Deschepper, Robin Dhooghe, Jason Dijkhuis, Jean-Sébastien Roy, and Ann Cools. Proprioception: How is it affected by shoulder pain? a systematic review. *Journal of Hand Therapy*, 33(4): 507–516, 2020.
- Mariangela Manti, Taimoor Hassan, Giovanni Passetti, Nicolò D’Elia, Cecilia Laschi, and Matteo Cianchetti. A bioinspired soft robotic gripper for adaptable and effective grasping. *Soft Robotics*, 2(3):107–116, 2015.
- Chang Li, Jie Fei, Enzhi Zhou, Rui Lu, Xiaohang Cai, Yewei Fu, and Hejun Li. Optimization of pore structure and wet tribological properties of paper-based friction materials using chemical foaming technology. *Friction*, 10(9): 1317–1334, 2022b.
- Chang Li, Yewei Fu, Beibei Wang, Wenhao Zhang, Yuanhe Bai, Leilei Zhang, and Lehua Qi. Effect of pore structure on mechanical and tribological properties of paper-based friction materials. *Tribology International*, 148:106307, 2020.
- Liwen Zhang, Huawei Chen, Yurun Guo, Yan Wang, Yonggang Jiang, Deyuan Zhang, Liran Ma, Jianbin Luo, and Lei Jiang. Micro–nano hierarchical structure enhanced strong wet friction surface inspired by tree frogs. *Advanced Science*, 7(20):2001125, 2020.